Chapter 6
Separation of Particles from a Gas

As the counterpart of Chap. 5, this chapter covers the basics behind various particulate emission control devices. It starts with a general introduction to particle separation efficiency followed by systematic introduction to the principles for gravity settling chambers, centrifugal separators (cyclones), electrostatic precipitators, and filters.

6.1 General Consideration

Particle separation is a critical step in many energy and environmental engineering applications. In addition to the reduction of particulate emission before a flue gas is discharged to atmosphere, particle separation is an important step for alternative fuel development. For example, in order to clean gaseous fuel from gasification, heavy gas molecules have to be removed from the stream using membranes. However, this cannot be achieved without the removal of particulate matter from the gas stream, otherwise the membrane will lose its function by clogging.

In general, a particle can be separated from its carrier gas by gravitational settling, cyclonic separation, filtration, wet scrubbing, thermal force separation, and electrical separators like electrostatic precipitators. The thermal force separators work in principle, but it is not effective in handling large volume of gas flow or for large particles [15], therefore, it will not be introduced in this book.

The performance of a particle separation device can be quantified by the following three main parameters: pressure drop, capability, and most importantly, efficiency.

6.1.1 Particle Separation Efficiency

The efficiency of a particle separator can be described by grade efficiency curve, which gives the separation efficiency as function of particle size. It can also be quantified by total efficiency.

Z. Tan, *Air Pollution and Greenhouse Gases*, Green Energy and Technology,
DOI 10.1007/978-981-287-212-8_6

Consider a particle separation device, which could be any of the devices to be introduced shortly. N_i and N_o are the numbers of particles with size d_p before and after the device, respectively. The total amount of particles collected by the device is $N_c = N_i - N_o$. Then the separation efficiency for particles with a size d_p is defined as the

$$\eta(d_p) = \frac{N_c}{N_i} = 1 - \frac{N_o}{N_i}. \tag{6.1}$$

The performance of a particle separation device can also be described with a penetration efficiency (P).

$$P(d_p) = \frac{N_i}{N_o}. \tag{6.2}$$

Obviously, the relationship between P and η is defined as

$$\eta = 1 - P \tag{6.3}$$

$\eta(d_p)$ represents the efficiency for the particles having same diameter, d_p. It is also referred to as grade collection efficiency.

An important parameter in fractional efficiency is the so-called "cut size", d_{50}, which is the particle size for which the separation efficiency is 50 %.

In air pollutant control, we deal with polydisperse particles. It leads to another term called total efficiency. The total efficiency by considering all the particles is

$$\eta = \frac{\int_0^\infty N_o(d_p)dd_p}{\int_0^\infty N_i(d_p)dd_p} = \frac{\int_0^\infty \eta_p(d_p)N_i(d_p)dd_p}{\int_0^\infty N_i(d_p)dd_p} \tag{6.4}$$

When the particle size distribution is measured using discrete data, it can be estimated by

$$\eta = \frac{\sum \eta(d_{pi})N_i(d_{pi})}{\sum N_i(d_{pi})} \tag{6.5}$$

If the particle density m is assumed to be the same before and after the device and all the particles with the same size have the same mass, we can replace number N with mass m; Eq. (6.4) becomes

$$\eta = \frac{\int_0^\infty \mathrm{m}_{po}(d_p)d(d_p)}{\int_0^\infty \mathrm{m}_{pi}(d_p)d(d_p)} = \frac{\int_0^\infty \eta(d_p)\mathrm{m}_{pi}(d_p)d(d_p)}{\int_0^\infty \mathrm{m}_{pi}(d_p)d(d_p)} \tag{6.6}$$

Similarly, when the particle size distribution is measured using discrete data, Eq. (6.5) can be rewritten as

$$\eta = \frac{\sum_i \eta(d_{pi}) m_{pi}(d_{pi})}{\sum_i m_{pi}(d_{pi})} \tag{6.7}$$

With the fractional efficiency curve of a device determined, the total efficiency for polydisperse particles can be calculated using above equation. In the following analyses, only fractional efficiency will be introduced to avoid duplication of work.

6.1.2 Particle Separation Efficiency of Multiple Devices

In engineering applications, usually more than one unit is employed in order to achieve high efficiency or to handle a great amount of air flow. The former is achieved by connecting more than one unit in serial and the latter in parallel. Consider k identical devices arranged in serial, the number of particles entering the ith unit is the same as that penetrating through the $(i - 1)$th unit. Then the penetration through all the k units is

$$P = \Pi P_i = P_1 P_2 \ldots P_k \tag{6.8}$$

And the corresponding efficiency is

$$\eta = 1 - P = 1 - P_1 P_2 \ldots P_k \tag{6.9}$$

In this analysis, we actually made a critical assumption that the particle separation efficiencies of the identical units are the same. In reality, it is actually invalid because the particle separation efficiency of a unit depends on the incoming particle concentration, which keeps decreasing when the units are connected in serial. Therefore, careful interpretation of this equation should be executed.

Example 6.1: General particle separation efficiency
A filter has an efficiency of 85 %. What is the total efficiency if two of them working in serial.

Solution
With a single filter efficiency of 85 %, the corresponding penetration efficiency is 15 %. For two filters in serial, the total efficiency is thereby

$$\eta = 1 - P_1 P_2 = 1 - 0.15 \times 0.15 = 0.9775$$

The total filtration efficiency is 97.75 %.

6.2 Gravity Settling Chambers

A gravity settling chamber was mainly used for the separation of large particles from the air stream. In practice, a gravity settling chamber is only effective for particles with a diameter of 50 μm or larger. As seen in Fig. 6.1, it classifies the particles by gravitational force. A consequential drawback of these devices is the large footprint. Depending on the gas velocity, a chamber can be designed to operate at laminar flow or turbulent flow.

6.2.1 Laminar Flow Model

Consider a gravity settling chamber with dimensions of height H, length, L and width W. A particle having diameter d_p enters the chamber as shown in Fig. 6.2. Under laminar flow condition, the trajectory of any particle should be a straight line. As it moves from left to the right together with the airflow at a speed of U, it settles at a terminal speed of v_{TS}. The concept of terminal settling speed was introduced above in Sect. 4.2.1.

If the particle barely touches the lower right edge of the chamber when it enters the chamber at a height H_c, then all the particles of the same size entering the chamber above H_c will penetrate through the chamber; those below H_c will be

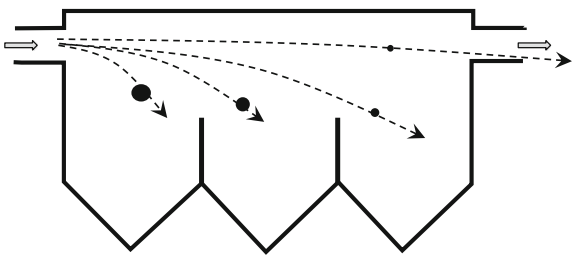

Fig. 6.1 A schematic diagram of a gravity settling chamber

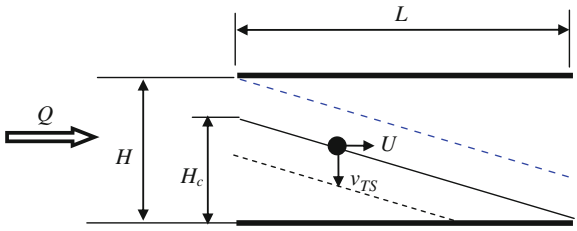

Fig. 6.2 A laminar flow gravity settling model

collected on the surface of the lower plate. This height H_c can be referred to as the critical height. Then the fractional efficiency of the chamber for this group of particles (d_p) is

$$\eta(d_p) = \frac{H_c}{H} \tag{6.10}$$

The time for a particle entering the chamber at the critical height, H_c, falls down through a vertical distance H_c while traveling a horizontal distance L, is

$$t = \frac{L}{U} = \frac{H_c}{v_{TS}} \tag{6.11}$$

It leads to

$$H_c = \frac{v_{TS}L}{U} \tag{6.12}$$

Substitute Eq. (6.12) into the efficiency Eq. (6.10) above, and we have

$$\eta(d_p) = \frac{v_{TS}L}{UH} \tag{6.13}$$

where the gas incoming speed can be determined from the flow rate of the air passing through the chamber,

$$U = \frac{Q}{WH} \tag{6.14}$$

where W is the width of the chamber. The terminal settling speed of a spherical particle falling in a gravitational field is

$$v_{TS} = \frac{\rho_p d_p^2 g C_c}{18\,\mu} \tag{6.15}$$

Therefore, the fractional particle separation efficiency can be described as

$$\eta(d_p) = \frac{\rho_p g d_p^2 C_c}{18\,\mu}\frac{LW}{Q} \tag{6.16}$$

6.2.2 Turbulent Flow Model

For turbulent flow model, we assume that the particles and the air are completely mixed at any cross section that is normal to the direction of airflow. Consider an element with an infinitesimal length dx. The concentration of particles within which is assumed to be uniform and the particles settle down at a terminal velocity of v_{TS}.

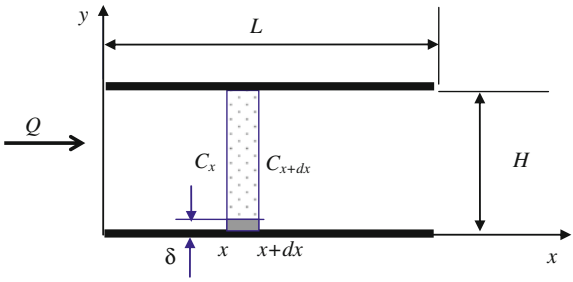

Fig. 6.3 A turbulent flow model of gravity settling chamber

During an infinitesimal period of time dt, the particles at the bottom of the chamber within a distance $\delta = v_{TS}\,\mathrm{d}t$ above the lower collecting plate are considered collected since only these particles can reach the surface (shaded area in the Fig. 6.3).

Then the amount of particles entering the element defined by dx equals to the total depositing on the bottom surface and that penetrating through the element, i.e.,

$$C_x UWH = Cv_{TS}W(\mathrm{d}x) + C_{x+\mathrm{d}x}UWH \tag{6.17}$$

The ratio of the amount of settled particles to the total amount of particles that enter the element defined by dx equals to the shaded area over the total elemental area, which gives

$$\frac{\mathrm{d}C}{C} = -\frac{v_{TS}}{H}\mathrm{d}t \tag{6.18}$$

The negative sign indicates the decreasing particle number concentration along x-direction.

Substitute the elemental residence time, $\mathrm{d}t = \mathrm{d}x/U$, into the above equation, and we have,

$$\frac{\mathrm{d}C}{C} = -\frac{v_{TS}}{HU}\mathrm{d}x \tag{6.19}$$

Integration of both sides leads to

$$\int_{C_i}^{C_o}\frac{\mathrm{d}C}{C} = -\int_0^L \frac{v_{TS}}{HU}\mathrm{d}x \tag{6.20}$$

We can get the penetration efficiency of the particles through the chamber

$$P = \exp\left(-\frac{v_{TS}L}{HU}\right) \tag{6.21}$$

The corresponding particle separation efficiency is thereby

$$\eta(d_p) = 1 - \exp\left(-\frac{v_{TS}L}{HU}\right) = 1 - \exp\left(-\frac{v_{TS}LW}{Q}\right) \tag{6.22}$$

It is important to note that in the analysis above, we assumed that a particle is collected and stays on the collection surface once it reaches there. This is actually more applicable to a sticky particle than a hard bumpy one. Particle bouncing and resuspension, also referred to as re-entrainment, introduced in Chap. 4, can significantly reduce the particle separation efficiency. Unfortunately, there is very limited knowledge about particle re-entrainment in particle separation due to its extreme complexity. terminal precipitating velocity,Therefore, the analytical formulae above, as those to come for other technologies, can only be used for guidance only.

Example 6.2: Gravity settling chamber efficiency
Consider a gravity settling chamber that is 1-m wide (W = 1 m) and 1-m high (H = 1 m). Air flow rate is 1 m^3/s (=3,600 m^3/h) and assume laminar flow within the chamber. Estimate its separation efficiency versus aerodynamic diameter under standard ambient condition.

Solution
Using Eq. (6.16), we can calculate the fraction efficiency for different particle size as follows:

$d_p(\mu m)$	$\eta(d_p) = \frac{\rho_p g d_p^2 C_c}{18\mu}\frac{LW}{Q}$ (%)
10	0.03
100	3
150	7
200	12
250	19
350	37
500	75
575	100

The fractional efficiency of a gravitational settling chamber is so low that it can no longer meet more and more stringent emission control requirements. As a result, there has been a sharp decline in the use of gravity settling chamber, although there are still a few of them in commercial use. However, similar analysis applies to electrostatic precipitator and, to a certain degree, to cyclone, which are introduced as follows.

6.3 Electrostatic Precipitation

The model analysis of electrostatic precipitation is very similar to that for the gravity settling chamber as discussed in Sect. 6.2 except that the driving force is now not gravitational but electrical. And the electrical field is arranged horizontal rather than vertical. Consider a flow through a pair of vertical plates H apart from each other with length L and depth b into the paper.

By replacing the gravitational settling velocity in Eq. (6.16) above with the terminal precipitating speed V_E, we can get the equation for laminar condition as follows:

$$\eta(d_p) = \frac{V_E L}{UH} = \frac{V_E Lb}{UHb} = \frac{V_E A}{Q} \quad \text{(Laminar)} \tag{6.23}$$

where A is the area of one plate collecting particles.

Following the similar analysis for gravitational setting chamber, we can also get the efficiency for complete mixing condition.

$$\eta(d_p) = 1 - \exp\left(-\frac{V_E A}{Q}\right) \quad \text{(Turbulent)} \tag{6.24}$$

where the terminal precipitating speed, V_E, in the electrical force field can be determined by equating the electrical force on the particles and the drag force,

$$qE = \frac{3\pi V_E d_p \mu}{C_c} \tag{6.25}$$

where q is the charge carried by the particles (columns) and E is the electric field intensity (V/m). This equation leads to

$$V_E = \frac{qEC_c}{3\pi d_p \mu} \tag{6.26}$$

Equation (6.26) shows that the precipitation speed of a particle depends on the charge carried by the particle, q, and the strength of the electrical field, E. They are determined as follows.

6.3.1 The Electric Field Intensity

The intensity of an electric field, E, is determined by the electrode geometry and the voltage difference that is applied between the electrodes.

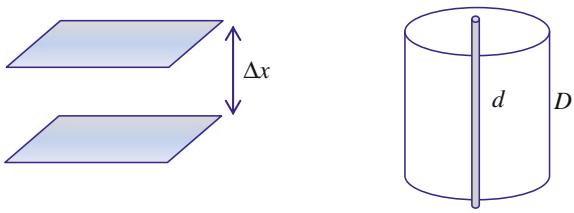

Fig. 6.4 Two typical electrode configurations

$$E = -\nabla V \tag{6.27}$$

where E is the electric field intensity in (V/m), V is the voltage. The exact form of the electric field depends on the configuration of the electrodes.

Two typical electrode configurations are shown in Fig. 6.4. One is parallel plates and another wire-tube. The difference in voltage between the two electrodes is V. Then the electrical field intensity between the two parallel plates is uniform and it is

$$E = \frac{V}{\Delta x} \tag{6.28}$$

However, for the wire-tube type, the electrical field intensity is a function of radial position, r,

$$E(r) = \frac{V}{r\ln(D/d)} \tag{6.29}$$

where d = diameter of the wire, D = diameter of the tube, and r = radial position, and $d/2 < r < D/2$

In reality, the electric field created by the electrode system may also be affected by the presence of electrons, ions, and other charged particles in the gas stream. This alters the electric field strength especially near the collection electrode.

6.3.2 Particle Charging

The success of ESP operation depends primarily on the charging of the particles. There are many ways to charge airborne particles, but only corona discharge can generate sufficient amount of ions for industrial electrostatic precipitators. Corona discharge is accomplished by applying high voltages in the order of kV on the discharge electrodes and grounding the collector plates. When the electric field intensity is greater than the electric breakdown intensity (typically about 30 kV/cm for ambient air), ions such as N^{2+} and O^{2+} and electrons, e^-, are produced at the electrode.

The particles can be charged by the ions generated by a corona discharger. There are two distinctive charging mechanisms, one being diffusive charging and another field charging. For either one, there is a saturation of charging because a particle can carry only certain amount of ions. With more and more ions charged on the particle, they also create another electric field preventing more ions from coming closer to the particle.

Ions charged to a particle can be positive, negative, or both. Depending on the polarity of the ions, the charging process is defined as unipolar or bipolar charging. Unipolar charging is much more effective than bipolar charging and thereby widely employed in industrial ESPs. Although there is not much difference between the effectiveness of positive and negative charging processes, positive charging will generate ozone, which is considered as secondary air pollutant. Therefore, negative charging is preferred and widely used.

6.3.2.1 Diffusive Charging

Airborne ions share the thermal energy of the gas molecules and obey the same law of kinetics theory. Diffusion of the ions in the air may result in collisions between the ions and the airborne particles, and thereby the attachment between the particles and the ions. This process is referred to as diffusive charging.

Consider an ion that is approaching a particle already being charged with n ions. The potential energy of the air with a distance r away from the particle is

$$P = \frac{K_E n e^2}{r} \tag{6.30}$$

where $K_E = 9 \times 10^9$ Nm^2/C^2 is a force constant.

According to White (1951), the spatial distribution of the concentration of airborne ions in a potential field is

$$N_i(r) = N_{i0} \exp\left(-\frac{P}{kT}\right) \tag{6.31}$$

where N_{i0} = ion concentration in the charging zone, k = the Boltzmann constant, T = absolute temperature in K, and P = potential energy in J.

Substitute Eq. (6.30) into (6.31), ion concentration near the particle at a radial distance of r becomes

$$N_i(r) = N_{i0} \exp\left(-\frac{K_E n e^2}{r}\frac{1}{kT}\right) \tag{6.32}$$

At the surface of the particle, where $r = d_p/2$, Eq. (6.32) leads to,

$$N_i(d_p/2) = N_{i0}\exp\left(-\frac{2K_E n e^2}{d_p kT}\right) \tag{6.33}$$

The number flux of ions can be determined by assuming that all the ions are captured when they strike the particle.

At $r = d_p/2$, the number of ions loss from the air to the surface of the particle is then described as

$$\frac{dn}{dt} = \frac{N_{i0}\bar{c}_i \pi d_p^2}{4}\exp\left(-\frac{2K_E n e^2}{d_p kT}\right) \tag{6.34}$$

where n is the number of ions moved from air to the surface of the particle, $\bar{c}_i$ = mean thermal speed of the ions and $(\pi d_p^2/4)$ stands for the surface area of the particle. Integration of the above equation leads the number of ions charged on the particles at time t

$$n(t) = \frac{d_p kT}{2e^2 K_E}\ln\left(1 + \frac{d_p K_E \bar{c}_i \pi e^2 N_{i0}}{2kT}t\right) \tag{6.35}$$

where $\bar{c}_i$ is the mean thermal speed of ions. Under normal condition, the mean thermal speed of ion $\bar{c}_i$ is about 239 m/s [41]. k is Boltzmann constant (1.38×10^{-23} J/K), $K_E = 9 \times 10^9$ Nm^2/C^2, and N_{i0} is ion concentration.

6.3.2.2 Field Charging

With the presence of electric field, ions are forced to move along the direction of the electric field. Leading to a high rate of collision between the ions and the particles. This is referred to as field charging mechanism. The number of ions charged to a particle by field charging depends on the properties of the particle, its size, and the intensity of the electric field, E:

$$n(t) = \frac{E d_p^2}{4eK_E}\left(\frac{3\varepsilon_r}{2+\varepsilon_r}\right)\left(\frac{t}{t+\tau}\right) \tag{6.36}$$

where E = intensity of the electric field with a typical value of 10^6 V/m, ε_r = relative permittivity or dielectric constant of the particle with respect to vacuum, and $\varepsilon_r = \varepsilon/\varepsilon_0$; $\varepsilon_0 = 8.854 \times 10^{-12}$ C/Vm is the permittivity of a vacuum. The permittivity of typical particles can be found in handbooks. τ is the charging constant and it varies with the field condition.

$$\tau = \frac{1}{\pi N_{i0} K_E e Z_e} \tag{6.37}$$

where Z_e = mobility of the ions, and the average value of the mobility of air ions is about 1.5×10^{-4} m^2/V s. A typical charging constant is $\tau = 0.01 - 0.1$ s using the above equation.

The number of ions that is eventually charged to a particle depends on charging time, the concentration of ions in the charging zone, and the electric mobility of these ions, which determines the moving speed of the ions in response to the electric field E. In a typical industrial application, the particle residence time t is of the order of 10 s. Therefore, $t \gg \tau$ and we can assume maximum field charging, which is from Eq. (6.36).

$$n_{\max} = \frac{E d_p^2}{4 e K_E} \left(\frac{3\varepsilon_r}{2 + \varepsilon_r} \right) \tag{6.38}$$

6.3.2.3 Combined Charging

Combined charging takes into consideration both charging mechanisms. The total number of ions charged to a particle is calculated using

$$n(t) = \frac{d_p kT}{2e^2 K_E} \ln\left(1 + \frac{d_p K_E \bar{c}_i \pi e^2 N_{i0}}{2kT} t \right) + \frac{E d_p^2}{4 e K_E} \left(\frac{3\varepsilon_r}{2 + \varepsilon_r} \right) \left(\frac{t}{t + \tau} \right) \tag{6.39}$$

On the right-hand side of the equation, the first term is for the effect of diffusive charging and the last for field charging. The relative importance of diffusive and field charging depends on the size of the particles to be charged. Since both diffusive and field charging are a function of d_p^2, which indicates that it is not the aerodynamic diameter but rather the actual surface area that affects the charging effect.

Figure 6.5 shows the relative importance of diffusive and field charging; calculation was based on the following parameters:

$K_E = 9 \times 10^9\ \mathrm{Nm^2/C^2}$	$Z_e = 1.50 \times 10^4\ \mathrm{m^2/Vs}$	$N_{io} = 5.00 \times 10^{14}\ \mathrm{ion/m^3}$
$e = 1.60 \times 10^{-19}\ \mathrm{C}$	$\bar{c}_i = 240\ \mathrm{m/s}$	$k = 1.38 \times 10^{-23}\ \mathrm{J/K}$
$T = 293\ \mathrm{K}$	$E = 1.0 \times 10^6\ \mathrm{V/m}$	$t = 0.1\ \mathrm{s}, \quad \varepsilon_r = 1$

It shows that diffusion charging is an important mechanism for particles smaller than 200 nm in diameter, whereas field charging dominates for particles larger than 2 μm.

In order to implement the charging mechanisms, diffusive, field, or both, there have to be enough ions generated. Among the ion generation technologies, corona discharge has been believed to be the most effective in producing sufficient ions. It has been well known that ozone and aerosol particles, especially smaller ones, are

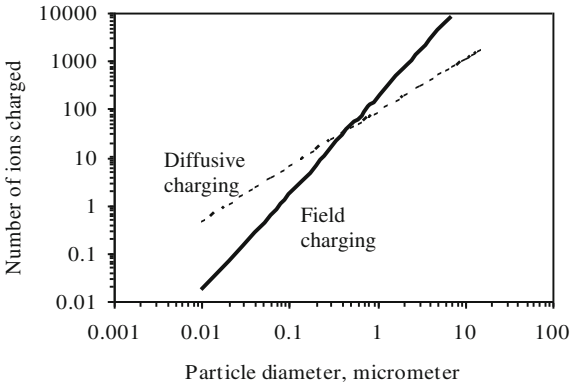

Fig. 6.5 Comparison of field and diffusive charging of particles

produced by corona discharge, and they are considered as secondary air pollutants. More information about nanoparticle generation in corona charger can be found in Chap. 14.

6.4 Cyclone

A cyclone separates particles from the air by "centrifugal force". As depicted in Fig. 6.6, particles and air enter the device from the side. When the air changes direction following the curvature of the device, particles tend to remain the same flow direction due to inertia. As a result, the particles move along radial direction with respect to the air. This is commonly referred to as centrifugal force, which is actually conceptually incorrect.

Figure 6.6 shows the top view of a cyclone body, the height and width of the rectangular inlet are H and W, respectively, and radii of the outer and inner tubes are

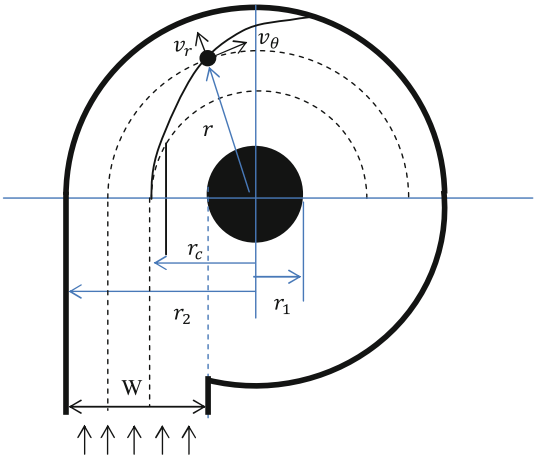

Fig. 6.6 Particle motion in rotating fluids

r_2 and r_1, respectively. Assume there is no leakage and the gas is incompressible, the flow rate Q is constant from the inlet through the annular chamber and the outlet.

6.4.1 Cyclone Fractional Efficiency

Assume the airflow within the cyclone is laminar. There is a critical radius, r_c, where a particle to be located at this position eventually reaches the inner surface of the outer body of the cyclone. Then, similar to the analysis for gravity settling chamber and electrostatic precipitator, the fractional particle separation efficiency is

$$\eta(d_p) = \frac{r_2 - r_c}{r_2 - r_1} = \frac{r_2 - r_c}{W} \tag{6.40}$$

At steady state, the average tangential velocity of the airflow is

$$\bar{u}_g = \frac{Q}{WH} = \frac{Q}{(r_2 - r_1)H} \tag{6.41}$$

With the laminar flow assumption, the airflow does not mix along the radial direction. The radial component of velocity of the particles can be derived from Newton's Second Law,

$$m_p \frac{\mathrm{d}v_r}{\mathrm{d}t} = F_C - F_D = 0 \tag{6.42}$$

where v_r is the radial speed of the particle. Assume a spherical particle with a density ρ_p and a diameter of d_p, the centrifugal force, F_C, and the drag force F_D exerted on the particle at any position r are, respectively

$$F_C = m_p \frac{v_\theta^2}{r} = \frac{\rho_p \pi d_p^3}{6} \frac{v_\theta^2}{r} \tag{6.43}$$

$$F_D = 8\,\pi \mu d_p v_r \tag{6.44}$$

In this equation, we ignored the Cunningham coefficient because cyclones are used primarily for separating particles with large sizes. In the Stokes region, $F_C = F_D$, and it leads to

$$v_r = \frac{\rho_p d_p^2 v_\theta^2}{18 \mu r} \tag{6.45}$$

It is commonly assumed that the particle follows air stream along tangential direction, that is, $v_\theta = u_\theta$. However, the exact description of air tangential speed u_θ depends on the researcher.

6.4.1.1 Crawford Model

Crawford [6] derived a formula by applying fluid dynamics to the air phase, which leads to

$$v_\theta = u_\theta = \frac{Q}{H \ln(r_2/r_1)} \frac{1}{r} \tag{6.46}$$

Substituting Eq. (6.46) into (6.45) leads to

$$v_r = \frac{\rho_p d_p^2}{18\mu} \left[\frac{Q}{H \ln(r_2/r_1)} \right]^2 \frac{1}{r^3} \tag{6.47}$$

Over an infinitesimal period of time, dt, the particle moves outward along radial direction a distance of d$r = v_r$dt and an arc length along the tangential direction, rd$\theta = v_\theta$dt. For the same dt

$$\mathrm{d}t = \frac{\mathrm{d}r}{v_r} = \frac{r\mathrm{d}\theta}{v_\theta} \tag{6.48}$$

It leads to

$$\frac{\mathrm{d}r}{r\mathrm{d}\theta} = \frac{v_r}{v_\theta} \tag{6.49}$$

Substituting Eqs. (6.46) and (6.45) into (6.49) leads to

$$\frac{r\mathrm{d}r}{\mathrm{d}\theta} = \frac{\rho_p d_p^2}{18\mu} \frac{Q}{H \ln(r_2/r_1)} \tag{6.50}$$

where the right-hand side of this equation is constant for fixed particle size and cyclone configuration. For a particle entering the cyclone at $r = r_c$ when $\theta = 0$, its radial position in the cyclone is defined by

$$r^2 - r_c^2 = \left[\frac{\rho_p d_p^2}{9\mu} \frac{Q}{H \ln(r_2/r_1)} \right] \theta \tag{6.51}$$

When the particle reaches the collecting wall, $r = r_2$, and the corresponding angle θ_2 is determined by

$$r_2^2 - r_c^2 = \left[\frac{\rho_p d_p^2}{9\mu} \frac{Q}{H \ln(r_2/r_1)} \right] \theta_2 \tag{6.52}$$

Substituting r_c back into Eq. (6.40) leads to the description of the fractional efficiency as

$$\eta(d_p) = \frac{r_2 - \left[r_2^2 - \frac{\rho_p d_p^2 Q \theta_2}{9\mu H \ln(r_2/r_1)}\right]^{1/2}}{r_2 - r_1} \tag{6.53}$$

It seems like we have now a mathematical description but it requires a certain calibration because θ_2 is unknown. In addition, it is unlikely that there is a laminar flow in an industrial scale cyclone. Alternatively, we can use the empirical model developed by Lapple [19] that follows.

6.4.1.2 Lapple Model

A semi-empirical model was developed by Lapple [19]. The average radial speed is described in terms of the migration time. It can be considered as the average terminal speed in the centrifugal field. On average, before the particle reaches the inner surface of the cyclone outer wall, corresponding to $r = r_2$, the average terminal speed is

$$v_r = \frac{r_2 - r_c}{t} \tag{6.54}$$

where t is the corresponding residence time. Combination of Eqs. (6.45) and (6.54) leads to

$$r_2 - r_c = \frac{\rho_p d_p^2 v_\theta^2}{18\mu r} t \tag{6.55}$$

Substituting Eq. (6.55) into (6.40) leads to the fractional efficiency of the particles with diameter d_p

$$\eta(d_p) = \frac{r_2 - r_c}{W} = \frac{\rho_p d_p^2 v_\theta^2}{18\mu r W} t \tag{6.56}$$

The residence time depends on the engineering design of the cyclone. Many models of commercial cyclones have been developed since the end of the nineteenth century. Typical cyclones are classified into four basic categories, as depicted in Fig. 6.7, based on airflow direction:

(1) reverse flow with a tangential inlet (involute),
(2) reverse flow with a guide vane inlet (vane-axial),
(3) uniflow with a tangential inlet, and
(4) uniflow with guide vanes.

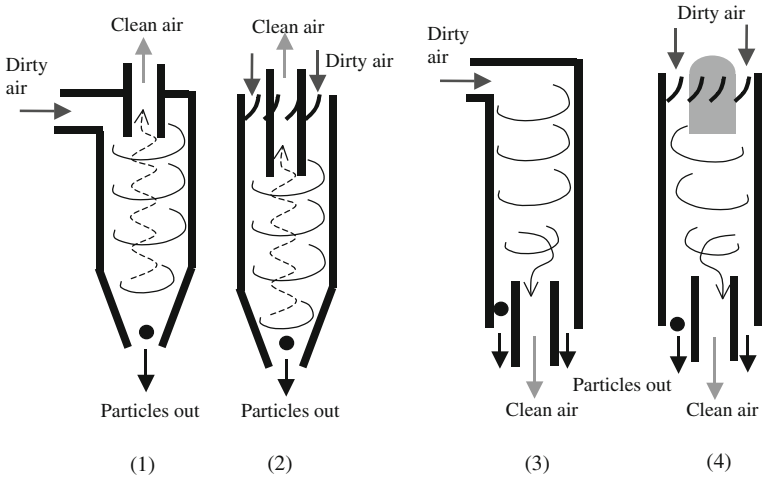

Fig. 6.7 Schematics of four types of cyclones (*Source* [42])

Our analysis continues with the mostly widely used cyclone model, involute cyclone. An involute cyclone is a conventional reverse flow cyclone that has been well standardized and commercialized. It can be classified into three types based on the flow rate capacity and efficiency: conventional cyclone, high efficiency cyclone, and high throughput cyclone.

For the widely used, so-called Lapple cyclones [19], design parameters are given in Fig. 6.8 and Table 6.1 [21] with a typical gas inlet velocity in the range of 15–30 m/s [4]. The values in Table 6.1 are for guidance only. Actual design may vary.

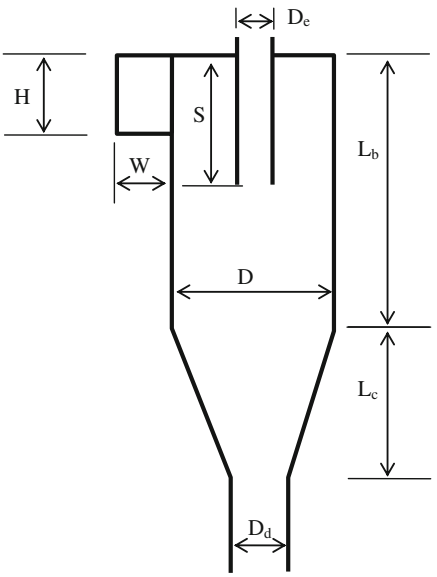

Fig. 6.8 Schematic diagram of a Lapple cyclone

Table 6.1 Design parameters for a Lapple cyclone

	High efficiency	Conventional	High throughput
Height of inlet, H/D	0.5–0.44	0.5	0.75–0.8
Width of inlet, W/D	0.2–0.021	0.25	0.375–0.35
Diameter of gas exit, D_e/D	0.4–0.5	0.5	0.75
Length of vortex finder, S/D	0.5	0.625–0.6	1.5–1.7
Length of body, L_B/D	1.4	1.75	1.7
Cone length, L_C/D	2.5	2	2.5–2
Diameter of dust outlet	0.375–0.4	0.25–0.4	0.375–0.4

The residence time of an involute cyclone is estimated by

$$t = \frac{\text{Circumference of the vortex} \times \text{Number of turns of the air}}{\text{Superficial gas speed}} \tag{6.57}$$

where the number of turns the gas flow makes before turning upward to the vortex finder (N_e) is

$$N_e = \frac{L_B + 0.5L_C}{H} \tag{6.58}$$

where L_B is the length of cyclone main body, and L_C is the length of the cyclone lower cone. Then the residence time can be calculated using

$$t = \frac{2\pi r N_e}{u_0} \tag{6.59}$$

Equation (6.56) then becomes

$$\eta(d_p) = \left(\frac{\pi N_e \rho_p}{9\mu W \bar{u}_g}\right) d_p^2 v_\theta^2 \tag{6.60}$$

If the average tangential speeds are approximated as the same, $v_\theta \approx u_\theta \approx \bar{u}_g$, then Eq. (6.60) becomes

$$\eta(d_p) = \left(\frac{\pi \bar{u}_g N_e \rho_p}{9\mu W}\right) d_p^2 \tag{6.61}$$

Instead of using this equation for direct calculation of the particle fractional efficiency, Lapple [19] presented a semi-empirical equation by introducing the cut size into the analysis. The corresponding cut size is first determined using Eq. (6.61) by letting $\eta = 0.5$

$$d_{50} = \left(\frac{4.5\mu W}{\pi N_e \bar{u}_g \rho_p} \right)^{1/2} \tag{6.62}$$

With the computed cut size above, the fractional efficiency of the cyclone is described as a function of particle size, d_p, and cut size, d_{50}:

$$\eta(d_p) = \frac{1}{1 + (d_{50}/d_p)^2} \tag{6.63}$$

Example 6.3: Cyclone efficiency
A conventional cyclone has a body diameter of 20 cm and other geometries are listed in the table as follows. It operates at an inlet volumetric flow rate of 360 m^3/h. Assume standard condition, plot its fractional efficiency curve versus particle aerodynamic diameter.

	Ratio
Height of inlet, *H*/*D*	0.5
Width of inlet, *W*/*D*	0.25
Length of body, L_B/D	1.75
Cone length, L_C/D	2

Solution
First, we calculate the dimension of the cyclone as follows:

	Dimension
Body diameter, *D* (m)	0.2
Height of inlet, *H*	0.1
Width of inlet, *W*	0.05
Diameter of gas exit, D_e	0.1
Length of body, L_B	0.35
Cone length, L_C	0.4

The number of turns from Eq. (6.58) is

$$N_e = \frac{L_B + 0.5L_C}{H} = \frac{0.35 + 0.5 \times 0.4}{0.1} = 5.5$$

The inlet area of this cyclone is

$$A = HW = 0.005\left(\mathrm{m}^2\right)$$

The average inlet air speed is then

$$\bar{u}_g = \frac{Q}{A} = \frac{360\ \frac{\text{m}^3}{\text{h}} \times \frac{1\,\text{h}}{3{,}600\,\text{s}}}{0.005\,\text{m}^2} = 20\,\text{m/s}$$

Cut size is determined using Eq. (6.62):

$$d_{50} = \left[\frac{9\mu W}{2\pi N_e \bar{u}_g (\rho_p - \rho_g)}\right]^{1/2} = \left[\frac{9 \times 1.81 \times 10^{-5} \times 0.05}{2\pi \times 5.5 \times 20(1000 - 1.21)}\right]^{1/2}$$
$$= 3.43 \times 10^{-6}\,\text{m} \quad \text{or} \quad 3.43\,\mu\text{m}$$

Then the fractional efficiency is determined by using Eq. (6.63):

$$\eta(d_p) = \frac{1}{1 + (d_{50}/d_p)^2}$$

The curve is shown in Fig. 6.9. This example shows that a typical cyclone works effectively for particles larger than a few micrometers.

Their separation efficiency is, however, limited to 90 % or so for a cyclone of reasonable size (diameters up to 1 m) with reasonable pressure drop, and the separation efficiency rapidly deteriorates for particles smaller than 10 μm.

In the example above, we did not use the vortex finder. Vortex finder is indirectly related to the performance of a cyclone. Agglomeration of particles at the inlet region is the result of stronger centrifugal forces on larger particles than on smaller ones, causing a "sweeping" effect. At the same time, particles may short-cut from the inlet to the gas outlet if the "vortex finder" does not penetrate deep enough into the cyclone.

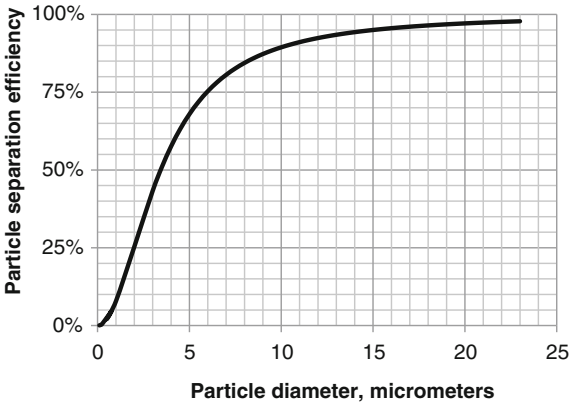

Fig. 6.9 Cyclone efficiency versus aerodynamic diameter

6.4.2 Pressure Drop of Cyclone

Pressure drop is the second important cyclone performance indicator, after collection efficiency. The pressure drop across a Lapple cyclone can be estimated by:

$$\Delta P = K\left(\frac{\rho_g \bar{u}_g^2}{2}\frac{HW}{D_e^2}\right) \tag{6.64}$$

which contains the design dimensions of H, W and D_e. For the coefficient K, a value in the range of 16–18 is suggested, with $K = 16$ as a recommended value [4].

A cyclone is capable of reducing dust concentrations in a gas stream from several g/m^3 to below 0.1 g/m^3. Cyclones can also be applied for removing water from oil at oil fields or solids from water. They are considered effective as low-cost preseparators for gas cleanup purposes.

6.4.3 Other Cyclone Models

Many analytical or semi-empirical models have been developed to predict the collection efficiencies of reverse flow cyclones under laminar or complete mixing assumptions. In these theoretical analyses, dimensionless geometric parameters are frequently defined. Dirgo and Leith [9] have summarized the models that were developed prior to 1985. It was stated that Lapple's cut-size theory based on time flight approach was widely cited in North American literature, while Barth's theory based on static particle approach was more often referred to in Europe. Both theories are based on laminar flow assumption. The well-known Leith–Licht model [22] developed in the 1970s was based on the assumption that flow was turbulent and uncollected particles were completely and uniformly mixed. Barth's theory and Leith–Licht theory were closest to Dirgo and Leith's experimental results [9] obtained from a Stairmand high efficiency cyclone.

Several uniflow cyclone models have been published too. Most researchers assume that increasing the separation length favors the solids separation efficiency, as the residence time increases allowing more particles to migrate to the wall of the cyclone. Summer et al. [32] reported an optimum separation length of around 1 cyclone diameter. Gauthier et al. [12] found that the optimum length increased with the inlet air velocity. These assumptions were validated by experimental results of large particle separation in a small uniflow cyclone with a tangential inlet. The diameter of the cyclone was 50 mm and the particles had a mean diameter of 29 μm. These models, however, might not apply for separation of fine particles in cyclones handling high airflow rates, where high turbulence exists.

Ogawa et al. [24] analyzed the separation mechanism of fine solid particles for a uniflow cyclone and demonstrated that particle cut size could be smaller than 5 μm. However, this theory is also based on small scale models. Their outer diameters

range from 30 to 99 mm and the lengths range from 90 to 279 mm. Furthermore, uniflow cyclones of commercial size suitable for large volume of air cleaning, especially those applicable for dusty airspaces, also need to be examined. Tan [33] derived a model for uniflow cyclone with tangential inlet and concentric exit.

Overall, cyclones are characterized with their simple structure, low cost, small footprint, and large capacity. Theoretically, high flow rate leads to higher particle separation efficiency. On the other hand, the most important contras of cyclones are high pressure drop, and relatively low efficiency for fine particles as demonstrated in Example 6.3. For reverse flow cyclones, the layer of collected particles may come in contact with the flow field of the gas, leading to re-entrainment. Most critical is the position near the bottom outlet for the collected dust, where the downward swirl turns upward into the inner vortex toward the gas outlet. At that point strong re-entrainment of collected particles may occur, which most certainly will leave the cyclone with the gas.

6.5 Filtration

Filtration is a process where particles are separated from a fluid using porous media called filter. Filtration is widely used for particle–fluid separation. Our focus here is air filtration, although similar principles apply to particle–liquid separation. For aerosol particles to be captured by a filter, they are first transported from the air to filter medium surface, and then collide with the surface. Particles cannot be captured by the filter unless they reach the surface of the filter media. However, successful transport does not ensure the particles being captured.

According to conventional particle dynamics, the collision between the particles and the filter surface may result in

- some particles adhere to the surface and they are considered removed from the air,
- other particles rebound from the surface and remain airborne.

The resultant filtration efficiency is thereby,

$$\eta = \eta_{ts} \times \eta_{ad} \tag{6.65}$$

where η_{ts} is the transport efficiency and η_{ad} is the adhesion efficiency. In classic filtration models, it is assumed that a particle is permanently removed from the gas stream once it reaches the filtration medium surface, i.e.,

$$\eta_{ad} \equiv 1 \tag{6.66}$$

Thereby, the filtration efficiency is the same as transport efficiency.

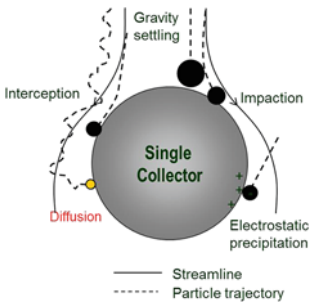

Fig. 6.10 Five particle transport mechanisms in filtration

$$\eta = \eta_{\text{ts}} \tag{6.67}$$

There are five basic particle *transport* mechanisms in filtration: interception, inertial impaction, diffusion, gravity settling, and electrostatic attraction. They are illustrated in Fig. 6.10. They are also applicable to particle filtration in liquid media and even particle feeding in biology [7]. While the method of analysis may be different for each specific case, the mechanisms are the same.

- *Interception*: Interception happens when a particle follows a gas streamline that comes within one particle radius to the surface of the filter media. The particle is captured because of its finite size. When interception dominates, it is assumed that the particles follow the streamlines perfectly, and they do not depart from the streamlines of the gas phase. This characteristic is unique and different from the other four mechanisms.
- *Inertial impaction*: When there is a sudden change in the flow direction near the media, a particle may be captured because of its inertia. This is referred to as *inertial impaction*. During an inertial impaction, the particle to be captured crosses the gas streamlines and reaches the surface of the filter media.
- *Diffusion*: Airborne particles can be captured by a surface due to the Brownian motion. This is especially true for small particles and also for the particles near the filter media surface.
- *Electrostatic attraction*: Electrostatic attraction takes place when the particles and the filter are charged. It follows the principle of particle dynamics in an electric field. The electrostatic attraction can be extremely important of all the mechanisms but is equally difficult to quantify because the charge on the particles or on the filters are often unknown. In most analytical works, electrostatic attraction is neglected due to the shortage of information.
- *Gravitational settling*: Gravitational settling takes place when a particle falls onto the filter during its motion. It is an inertial separation process. It is effective only for large particles or in air moving at low speed.

Filtration theory is essentially concerned with the prediction of the particle collection efficiency and the pressure drop as the carrier gas passes through the filter. Theoretically, they can be accurately calculated if the gas flow within a filter

could be mathematically described precisely. However, the random orientations of the filter media, especially the fibers within a filter, make it nearly impossible to achieve accurate mathematical solution. Instead, simplified filtration models are introduced as follows.

6.5.1 Single Fiber Filtration Efficiency

The simplest model consists of an isolated cylinder (simulating a single fiber) or a hole (for single pore) or a sphere (simulating a granule) in an otherwise undisturbed flow of fluid (gas or liquid). This may be justified for perfectly designed filters with excessively high porosity. Although the model based on isolated filter medium has been quite useful in illustrating the relative importance of different transport mechanisms, it is challenging to relate the rate of particle deposition on an isolated medium to the collection efficiency of a real filter that is filled with random fibers or granules.

A better approach, although still quite far from being realistic, is the model based on Kuwabara [18] cell model of forces experienced by randomly distributed parallel circular cylinders or spheres in a viscous flow at small Reynolds number. This cell model has been used by several researchers as a starting point for their filtration models, especially for fibrous filter models. Unlike the isolated cylinder or sphere models, these newer models address the influence of the surrounding filter media. However, the Kuwabara model and its modified versions still have limitations because they cannot be justified. Kirsh and Fuchs [17] developed a 3D model to represent a real filter more closely than earlier models; this model is too complicated to be solved easily. Therefore, we will not discuss it.

Yeh and Liu [38, 39] developed a model of flow over a staggered array of cylinders (Fig. 6.11) to investigate Kuwabara's model with slip effect taken into consideration. With this they quantified the effects of inertial impaction, diffusion, and interception. These models were also experimentally validated [38, 39]. And,

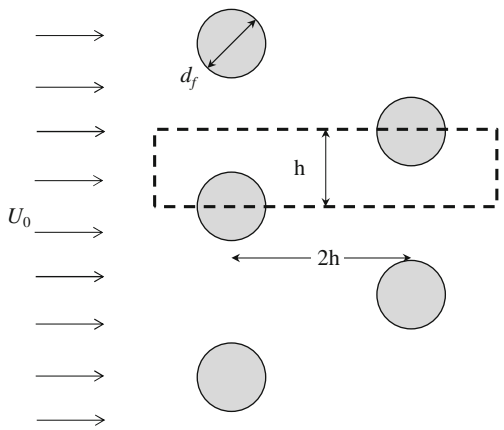

Fig. 6.11 Staggered array filter model

later on, the equations for diffusion and interception were further simplified by Lee and Liu [20]. Our discussion is focused on the staggered array models as follows.

In the staggered array model, air approaches the cylinders with a uniform speed of U_0. The diameter of the uniform cylinders is d_f. In the cylindrical coordinates defined by (r, θ) with origin at the center of the cylinder, the corresponding dimensionless stream line function is

$$\begin{aligned} \Psi &= \frac{\sin\theta}{2Y}\left[\frac{A}{r^*} + Br^* + 2r^*\ln r^* - \frac{\alpha}{2}(r^*)^3\right] \\ A &= \frac{\left(1-\frac{1}{2}\alpha\right)\left(1-Kn_f\right)+\alpha Kn_f}{1+Kn_f} \\ B &= \frac{(1-\alpha)\left(Kn_f-1\right)}{1+Kn_f} \end{aligned} \tag{6.68}$$

where α is called the solidity of the filter, it is the ratio of solid volume to the entire filter bulk volume; $r^* = 2r/d_f$ is a dimensionless distance from the center of the fiber; the hydrodynamic factor Y is described as

$$Y = -\frac{\ln\alpha}{2} - \frac{3}{4\left(1+Kn_f\right)} + \frac{\alpha}{1+Kn_f} + \frac{Kn_f(2\alpha-1)^2}{4\left(1+Kn_f\right)} - \frac{\alpha^2}{4} \tag{6.69}$$

In this equation, the Knudsen number is defined as the ratio of the mean free path of the gas molecules to the radius of the filter fiber. Similar to Eq. (4.8), it is expressed as

$$Kn_f = 2\lambda/d_f \tag{6.70}$$

It quantifies the slip effect in particle filtration; Kn_f is significant for $d_f < 2$ μm. The mean free path of air (λ) under standard conditions is about 0.066 μm. In this case, $2\lambda/d_f < 0.066$ % when $d_f > 2$ μm.

For cases with $\alpha \ll 1$ and $Kn_f \ll 1$, the streamline function becomes

$$\Psi = \frac{\sin\theta}{2Y}\left(\frac{1}{r^*} - r^* + 2r^*\ln r^*\right) \tag{6.71}$$

For a typical filtration process under normal conditions, $Kn_f \ll 1$, and the Kuwabara hydrodynamic factor in Eq. (6.69) can be simplified by letting $Kn_f \to 0$:

$$Y = -\frac{\ln\alpha}{2} - \frac{3}{4} + \alpha - \frac{\alpha^2}{4} \tag{6.72}$$

In certain special filtration processes such as those under low pressure or those with very fine filter diameter, Eq. (6.69) should be used for a great accuracy in calculation.

The single fiber filtration efficiency by inertial impaction per unit length of fiber due to inertial *impaction* is calculated as

$$\eta_{\text{ip}} = \left(\frac{Stk_m}{2Y}\right) I \tag{6.73}$$

where I is described as

$$I = \begin{cases} \left(29.6 - 28\alpha^{0.62}\right)R^2 - 27.5R^{2.8} & \text{for } R < 0.4 \\ 2 & \text{for } R \geq 0.4 \end{cases} \tag{6.74}$$

There is no simple equation for I when $R \geq 0.4$. As an approximation, a value of $I = 2.0$ for $R \geq 0.4$ can be used.

In these equations, R is called the interception parameter and it is defined as ratio of particle diameter d_p to the filter fiber diameter d_f:

$$R = \frac{d_p}{d_f} \tag{6.75}$$

Stk_m is the modified Stokes number defined by the particle Stokes number with $d_c = d_f$ (Eq. (6.76)) divided by the hydrodynamic factor, Y

$$Stk = \frac{\rho_p d_p^2 C_c U_0}{18\mu d_f} \tag{6.76}$$

$$Stk_m = \frac{Stk}{2Y} \tag{6.77}$$

The single fiber efficiency due to diffusion per unit length of fiber is described as

$$\eta_{\text{D}} = \frac{3.65(Pe_m)^{-\frac{2}{3}} + 0.624(Pe_m)^{-1}}{2Y} \tag{6.78}$$

where Pe_m is the modified Peclet number. Similar to the modification to Stokes number, the modified Peclet number is

$$Pe_m = \frac{Pe}{2Y} \tag{6.79}$$

and the Peclet number is

$$Pe = \frac{U_0 d_f}{D_p} \tag{6.80}$$

where U_0 is the air velocity approaching the filter fiber, and D_p is particle diffusion coefficient that can be calculated using Eq. (6.81).

$$D_p = \frac{kTC_c}{3\pi\mu d_p} \tag{6.81}$$

Peclet number shows the effect of convective transport over diffusive transport of particles.

Later on, Lee and Liu [20] further simplified the Eq. (6.78) for diffusion as,

$$\eta_{\mathrm{D}} = 2.6\left(\frac{1-\alpha}{Y}\right)^{1/3} \quad Pe^{-2/3} \tag{6.82}$$

This simplified equation shows that $\eta_D \propto Pe^{-2/3}$ for a filter with a fixed solidity.

A general equation for single fiber filtration by *interception* can be described as (Lee and Liu [20], p. 152)

$$\eta_{\mathrm{it}} = \frac{1+R}{2Y}\left[2\ln(1+R) - (1-\alpha) + \left(1-\frac{\alpha}{2}\right)(1+R)^{-2} - \frac{\alpha}{2}(1+R)^2\right] \tag{6.83}$$

Equation (6.83) is a complete expression based on Kuwabara flow fields with a wide range of R and α. Simpler forms are given by Lee and Liu [20], p. 152 with limitations. The respective simplified equations for the cases $R \ll 1$ or $\alpha \ll 1$ are as follows:

$$\eta_{\mathrm{it}} = \frac{(1-\alpha)}{Y}\frac{R^2}{1+R} \quad \text{for } R \ll 1 \tag{6.84}$$

$$\eta_{\mathrm{it}} = \frac{2(1+R)\ln(1+R) - (1+R) - (1+R)^{-1}}{2Y} \quad \text{for } \alpha \ll 1 \tag{6.85}$$

6.5.1.1 Electrostatic Attraction

In most filtration models, electrical attraction is ignored, not because of its little importance, but rather the complex in the quantification of its effect. Nonetheless, Brown [3] gave a review of the theory of particle separation by electrostatic attraction. He introduced the single fiber efficiency for a neutral fiber and a particle with charge q as

$$\eta_{\mathrm{E}} = 1.5\left[\left(\frac{\varepsilon_r - 1}{\varepsilon_r + 1}\right)\right]\frac{q^2}{12\pi\mu U_0 \varepsilon_0 d_p d_f^2} \tag{6.86}$$

where ε_r = relative permittivity of the fiber and ε_0 = permittivity of a vacuum. Note that this equation was validated with the experimental measurements using glass fiber filters.

As introduced in Sect. 6.2, gravitational settling is not effective for micron particles, and it works only for large particles. Similarly, it does not play an important role in filtration compared to other mechanisms. We will skip its analytical solution.

6.5.1.2 Total Efficiency of a Single Fiber

With the filtration efficiency of each mechanism determined, the total efficiency of a single fiber per *unit length* is

$$\eta_{\mathrm{sf}} = 1 - (1 - \eta_{\mathrm{it}})\left(1 - \eta_{\mathrm{ip}}\right)(1 - \eta_{\mathrm{D}})(1 - \eta_{\mathrm{E}}) \tag{6.87}$$

In the computation of each component, the value should be less than or equal to 1.0.

Although each of the five filtration mechanisms plays a role in many cases, their relative importance is size dependent. As shown in Fig. 6.12, the contribution of diffusion drops with the increase of the particle diameter, whereas the effects of other mechanisms increase with particle diameter.

Example 6.4: Filtration efficiency based on different mechanisms
A fiber filter has a solidity of 3 %. The average diameter of the fiber is 5 μm. Estimate the single fiber efficiency based on, interception, impaction, and diffusion, respectively, when the face velocity is 0.05 m/s.

Solution
In this example, the following parameters are considered as constant

$$d_f = 5\,\mu\mathrm{m}, \quad \alpha = 0.03, \quad Kn_f = \frac{2\lambda}{d_f} = \frac{2(0.066)}{5} = 0.0264$$

$$Y = -\frac{\ln\alpha}{2} - \frac{3}{4} + \alpha - \frac{\alpha^2}{4} = 1.033, \quad \mu = 1.81 \times 10^{-5}\,\mathrm{Pa\,s}$$

The following variables can be calculated in an Excel sheet for different particle diameters

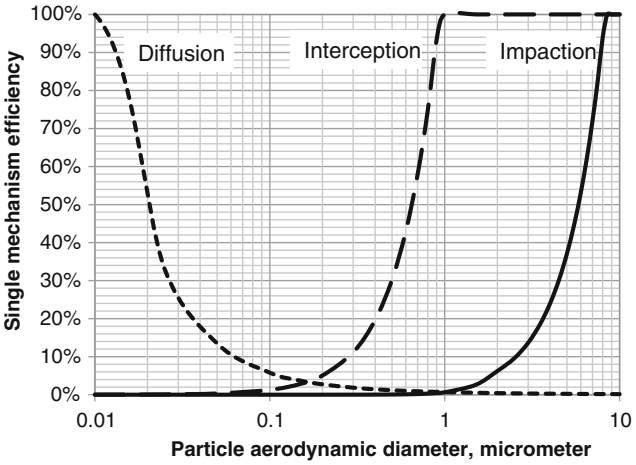

Fig. 6.12 Relative importance of different filtration mechanisms

$$R = \frac{d_p}{d_f}, \quad Stk_f = \frac{\rho_p d_p^2 C_c U_0}{18\mu d_f}, \quad Stk_m = \frac{Stk}{2Y}$$

$$I = \begin{cases} \left(29.6 - 28\alpha^{0.62}\right)R^2 - 27.5R^{2.8} & \text{for } R < 0.4 \\ 2 & \text{for } R \geq 0.4 \end{cases}$$

$$D_p = \frac{kTC_c}{3\pi\mu d_p}, \quad Pe = \frac{U_0 d_f}{D_p}, \quad Pe_m = \frac{Pe}{2Y}$$

The single fiber filtration efficiency by inertial interception, impaction, and diffusion, *per unit length* of fiber is calculated using

$$\eta_{\text{it}} = \frac{1+R}{2Y}\left[2\ln(1+R) - (1-\alpha) + \left(1-\frac{\alpha}{2}\right)(1+R)^{-2} - \frac{\alpha}{2}(1+R)^2\right]$$

$$\eta_{\text{ip}} = \frac{I}{2Y} Stk_m$$

$$\eta_{\text{D}} = \frac{3.65(Pe_m)^{-\frac{2}{3}} + 0.624(Pe_m)^{-1}}{2Y}$$

The curves are plotted in Fig. 6.12. As indicated in the figure, when all other conditions are the same, diffusion is dominating for small particles. However, its effectiveness also drops at high air speed. It can be easily seen by repeating the example by changing face velocity with U_0 = 0.1 m/s.

As shown in Fig. 6.12, one filtration mechanism often predominates over the other for certain size group. In general, interception and impaction are negligible for small particles, but they become important for particles larger than 1 μm in

diameter. Diffusion is the only important mechanism for particles below 0.2 μm, but drops quickly with the increase of particle diameter. The total efficiency is at the bottom for particles around 0.2 μm. This is because this group of particles is too large for diffusion and too small for impaction or interception to be effective.

6.5.2 Overall Fibrous Filtration Efficiency

Eventually we need to quantify the overall efficiency of an actual filter. "Overall filtration efficiency" is used here to avoid the confusion with the term "total efficiency" that has been used above to describe the total efficiency of a single fiber, Eq. (6.87). The overall filtration efficiency, η, can be derived from the total single fiber efficiency, η_{sf}, by the following simplified one-dimensional analysis.

As depicted in Fig. 6.13, analysis of overall filtration efficiency, consider a filter with a bulk thickness of L along x-direction, which is also the face velocity direction. The filter is filled with homogeneous fibers of diameter, d_f, and the length of the uniform single fiber is denoted as ds_f. Within an elemental thickness of dx, the solidity, α, from its definition is,

$$\alpha = \frac{\left(\pi d_f^2 \Big/ 4\right) \times ds_f}{A_c \times \mathrm{d}x} \tag{6.88}$$

where A_c is the bulk cross section area of the filter that is normal to the face velocity. It can be determined by the air flow rate

$$A_c = \frac{Q}{U_\infty} \tag{6.89}$$

where U_∞ is the bulk face speed, or the air speed approaching the filter. It is less than that approaching the fiber within the filter, U_0, because of the existence of solid fibers

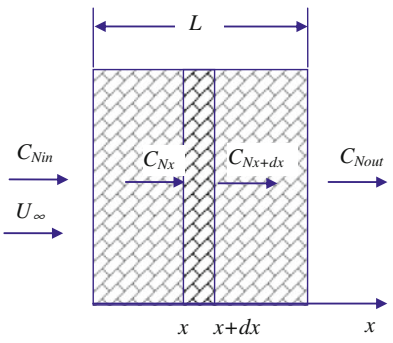

Fig. 6.13 Analysis of overall filtration efficiency

$$U_0 = \frac{U_\infty}{1-\alpha} = \frac{Q}{(1-\alpha)A_c} \tag{6.90}$$

The number concentration of particles lost per unit volume from the bulk air over the distance dx equals to that captured by the fiber with a single fiber efficiency η_{sf} corresponding to an approaching flow rate of $U_0 d_f \times ds_f$, where $d_f \times ds_f$ defines the cross section area of the fiber with the length of ds_f and the diameter of d_f.

$$Q \times dC_N(x) = -\eta_{\mathrm{sf}} C_N(x) U_0 d_f \times ds_f \tag{6.91}$$

where C_N is the number concentration of particles (#/m^3), the single fiber efficiency η_{sf} is determined by Eq. (6.87).

The LHS stands for the decrease in particle number per unit time after air passes through the bulk filter thickness dx, whereas the RHS stands for the reason of this decrease calculated as if all these particles passed through a single fiber with a cross section area of $\left(d_f \times ds_f\right)$ with an approaching speed of U_0 and a single fiber efficiency of η_{sf}. Equations (6.88) and (6.91) give,

$$\begin{aligned} A_c U_\infty \times dC_N(x) &= -C_N(x)\eta_{\mathrm{sf}} U_0 d_f \times \frac{4\alpha A_c \times \mathrm{d}x}{\pi d_f^2} \\ \frac{dC_N(x)}{C_N(x)} &= -\left(\frac{U_0}{U_\infty}\frac{\eta_{\mathrm{sf}} 4\alpha}{\pi d_f}\right)\mathrm{d}x \end{aligned} \tag{6.92}$$

Consider Eq. (6.90), we have

$$\frac{dC_N(x)}{C_N(x)} = -\left[\frac{\eta_{\mathrm{sf}} 4\alpha}{(1-\alpha)\pi d_f}\right]\mathrm{d}x \tag{6.93}$$

At any instant, all the parameters in the bracket on the right-hand side are constants for the particle size of d_p, which allows us to integrate from inlet to outlet of the filter:

$$\int_{C_{Ni}}^{C_{No}} \frac{dC_N(x)}{C_N(x)} = \int_0^L -\left[\frac{\eta_{\mathrm{sf}} 4\alpha}{(1-\alpha)\pi d_f}\right]\mathrm{d}x \tag{6.94}$$

which gives the overall fractional penetration through the filter

$$P\left(d_p\right) = \frac{C_{No}}{C_{Ni}} = \exp\left[\frac{-\eta_{\mathrm{sf}} 4\alpha L}{(1-\alpha)\pi d_f}\right] \tag{6.95}$$

Consequently, we can get the overall fractional filtration efficiency of the filter as

$$\eta(d_p) = 1 - \exp\left[\frac{-\eta_{sf} 4\alpha L}{(1-\alpha)\pi d_f}\right] \tag{6.96}$$

Equation (6.96) shows that we can calculate the fractional efficiency of a filter with fixed specifications (α, d_f, L) as long as the single fiber efficiency is determined. This equation also shows that the overall filtration efficiency increases over time as the solidity increases too when particles take more void space in filter.

Example 6.5: Filtration total efficiency
A filter is made of fiberglass with a solidity of 3 %, and it is 2 mm thick. The average diameter of the fiber is 5 μm. When the face velocity is 0.05 m/s, estimate its overall fractional filtration efficiency as a function of particle aerodynamic diameter under standard conditions (consider only interception, impaction, and diffusion).

Solution
Following the approach in Example 6.4, we can get the same single mechanism filtration efficiency for interception, impaction, and diffusion.

Then the single fiber total filtration efficiency per unit length of fiber is calculated using Eq. (6.87)

$$\eta_{sf} = 1 - (1-\eta_{it})(1-\eta_{ip})(1-\eta_D) \tag{6.97}$$

and the overall filtration efficiency of the filter itself is calculated using Eq. (6.96)

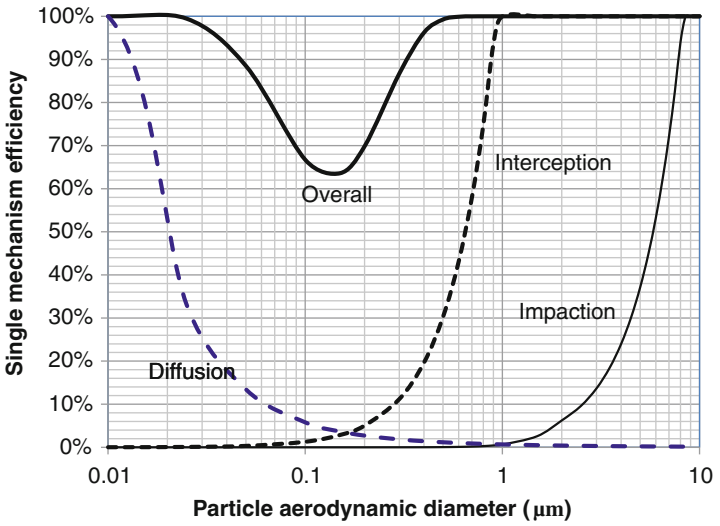

Fig. 6.14 Calculated overall filter efficiency versus particle aerodynamic diameter

$$\eta(d_p) = 1 - \exp\left[\frac{-\eta_{sf} 4\alpha L}{(1-\alpha)\pi d_f}\right] \tag{6.98}$$

The results are shown in Fig. 6.14.

Up to this point we assumed that filter fibers are oriented normal to the incoming air flow. It is clearly not the case in most engineering applications. Fiber orientation also affects the filtration efficiency and resistance to the air flow. The overall filtration efficiency is affected by the three-dimensional randomness of the fiber orientations too [31]. A filter with fibers randomly arranged in planes perpendicular to the approaching air velocity is more efficient than a filter with fibers randomly arranged in three dimensions.

The other assumptions in the preceding analysis of fibrous filtration are that all the aerosol particles are spherical and that the adhesion efficiency is 100 %. These simplifications do not introduce much of error because the likelihood of an aerosol particle adhering to a fibrous filter depends on not only the air flow velocity but also the particle–filter interfacial characteristics. Nonspherical particles are more likely to be captured than spherical ones. And, functions that correct for imperfect adhesion can be empirically derived for particular cases.

6.5.3 Fibrous Filter Pressure Drop

The pressure drop across a fiber filter is caused by the combined effect of each fiber resisting the flow of air past it. Davies [8] defined a dimensionless filter pressure coefficient as

$$C_{\Delta P} = \frac{\Delta P}{4\mu U_0 L \Big/ d_f^2} \tag{6.99}$$

With a known pressure drop coefficient, the pressure drop can be calculated as

$$\Delta P = C_{\Delta P} \frac{4\mu U_0 L}{d_f^2} \tag{6.100}$$

By dimensionless analysis and experimental correlation, Davies [8] obtained $C_{\Delta P}$ as a function of solidity in the range of 0.06–0.3 as follows,

$$C_{\Delta P} = 16\alpha^{1.5}\left(1 + 56\alpha^3\right) \tag{6.101}$$

Combination of Eqs. (6.100) and (6.101) leads to the total pressure drop over a bulk filter as

$$\Delta P = \frac{64\mu L U_0}{d_f^2}\alpha^{1.5}\left(1 + 56\alpha^3\right) \tag{6.102}$$

where the pressure drop ΔP is in Pascal. It is thus directly proportional to thickness of the filter L and inversely proportional to cross section area of the fiber d_f^2.

From the staggered array model, Yeh and Liu [38, 39] calculated the drag force over the fibers as

$$F_D = \frac{4\pi\mu U_0}{Y} \tag{6.103}$$

and the corresponding *pressure drop per unit thickness* of the filter is

$$\Delta P' = \frac{16\mu\alpha U_0}{Y d_f^2} \tag{6.104}$$

Then the total pressure drop over the entire array is determined as

$$\Delta P = L\Delta P' = \frac{16L\mu\alpha U_0}{Y d_f^2} \tag{6.105}$$

The corresponding pressure drop coefficient can then be determined by comparing Eq. (6.105) with (6.100).

$$C_{\Delta P} = \frac{4\alpha}{Y} \tag{6.106}$$

With Y in the denominator, Yeh's equation is complicated in form. In addition, as seen in Fig. 6.15, Yeh's model gives greater pressure drops than Davies model.

Figure 6.15 is produced for a filter with d_f = 10 μm, U_∞ = 0.2 m/s for α = 0.0–0.10 and L = 5, 10, 20 mm.

First of all, the pressure drop increases with filter solidity; the relationship based on these equations is not linear, so the pressure drop begins to dramatically increase as solidity increases. Increasing the thickness of the filter also causes the pressure drop to increase, but this increase is linear as the factor for thickness is not raised to any exponent and acts as a scalar quantity in the relationship (thus, this would also be true for velocity). Both of these responses make intuitive sense, as logically one would expect that the addition of filter material (whether by increasing solidity or thickness) would increase the pressure drop.

When comparing these two different models, it is clear that, for the same filter and operating conditions, Yeh's equations predict a greater pressure drop. Yeh's equations predict pressure drops about 1.5 times higher than Davies's. When solidity is 1 (though, this may be outside of the equation's domain), the result of

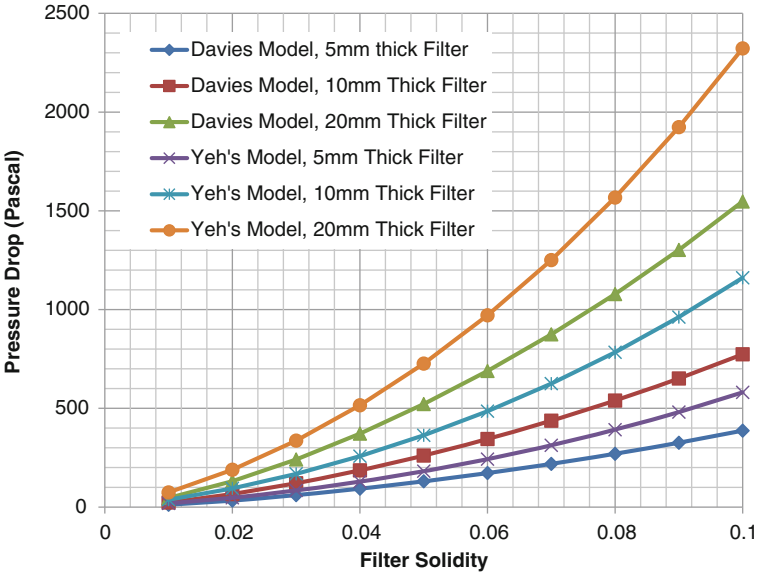

Fig. 6.15 Comparison between Yeh's and Davies models

$$Y = -\frac{\ln(\alpha)}{2} - \frac{3}{4} + \alpha - \frac{\alpha^2}{4}$$

evaluates to zero, and the pressure drop is infinite because the filter is completely blocked; a situation that Davies's model cannot predict.

Actually both models overestimate the pressure drop of a fibrous filter, but Davies's model is closer to experiments and therefore more widely used.

6.5.4 Particle Accumulation

A factor that is not considered so far in the preceding analysis is the effect of particle buildup on the fiber surface as the particle collection proceeds. Particles buildup on the fiber surface and it can be within the filter or on the surface of the filter, depending on the solidity of the filter and the particle sizes. The smaller the particle sizes, the deeper it goes into the bulk filter, and these particles are captured by internal fibers. This type of filter is also called internal filter. Larger particles are captured on the surface and these particles form a layer of dust, which are commonly called dust cake in industry. Since surface filters are designed to collect particles on the surface, they are usually as thin as a piece of fabric cloth. Surface filters can be reused after removal of the dust cake.

The buildup of particles inside and/or on a filter surface results in more or less structural changes in the filter and consequently alters the filtration efficiency and its resistance to flow. These particles deposited on the filter surface can themselves act as filter media. These factors should be taken into consideration in engineering design and practices. And it is discussed in Chap. 10, Sect. 10.2.2.

6.5.5 Granular Filtration

When the filter media is made of granules rather than fibers, the corresponding filters are called granular filters. It can be considered as an internal filter with respect to a pack of granules or surface filter with respect to each single layer. The earliest application of granular filtration was for water treatment. Layers or deep beds of solid granules (e.g., sands) have been used for a long time for precleaning drinking water. Recently, it has been tested for air emission control, especially for high-temperature applications. Low-cost granules such as sand, silicate, or alumina gravel can function very well at temperatures of as high as 450–500 °C. However, at higher temperatures, sintering of the granules and fine particles on granules may take place, leading to extreme filter clogging.

Granular filtration model was mainly based on the numerical analysis by Rajagopalan and Tien [30] predicting the trajectories of the particles moving around the filter granules under various conditions. By taking advantage of regression analysis, they developed the classic Rajagopalan–Tien model, referred to as RT-model hereby. Similar to the single fiber analysis, a single granule also captures aerosol particles by diffusion, interception, sedimentation efficiency, and electrostatic precipitation (ESP).

Starting from the single granule analysis, they derived the total filtration efficiency of a granular column filled with uniform granules. The correlation between the single granule efficiency and the overall packed bed efficiency is

$$\eta(d_p) = 1 - \exp\left[-1.5 f \alpha \eta_{sG} \left(\frac{h}{d_G}\right)\right] \tag{6.107}$$

where f is an empirical fitting factor, representing the fraction of contacts between particles and collector granules; η_{sG} is the single granule efficiency; h is the height of the packed bed filled with granules; α is the filter solidity that depends on d_G, the diameter of the granules.

The internal pores of the individual granules are disregarded in the equations. The average bed solidity can be determined using the equations proposed by Pushnov [27].

$$\alpha = \begin{cases} 1 - \left[a\left(\frac{d_{\text{bed}}}{d_G}\right)^{-n} + b\right] & \text{for } \frac{d_{\text{bed}}}{d_G} > 2 \\ 1 - 12.6\left(\frac{d_{\text{bed}}}{d_G}\right)^{6.1} \exp\left(-\frac{3.6 d_{\text{bed}}}{d_G}\right) & \text{for } \frac{d_{\text{bed}}}{d_G} < 2 \end{cases} \tag{6.108}$$

where d_{bed} = body diameter of packed bed. The coefficients of a, b, and n are constants and dependent on the shape of the granules. For *spherical* granules,

$a = 1,\ b = 0.375$ and $n = 2$

By ignoring the ESP effect, the filtration efficiency of *a single granule* is described in terms of several dimensionless variables as

$$\eta_{\text{sG}} = 4A_s^{1/3}\left(\frac{D_p}{U_0 d_G}\right)^{2/3} + A_s N_{\text{vdw}}^{1/8}\left(\frac{d_p}{d_G}\right)^{15/8} + 3.38 \times 10^{-3} A_s Gr^{1.2}\left(\frac{d_p}{d_G}\right)^{-0.4} \tag{6.109}$$

where D_p = particle diffusion coefficient, U_0 = approaching air speed, d_G = granule diameter, d_p = particle diameter, Gr = gravity number, which is defined as the ratio of gravity settling speed to approaching air speed, N_{vdw} = van der Waals number, and A_s = filter porosity parameter. The first term on the right-hand side characterizes the diffusion effect, second term for van der walls effect, and the last term for gravitational effect.

With the definition of gravity settling speed defined in Eq. (6.110)

$$v_{\text{TS}} = \frac{\rho_p d_p^2 g C_c}{18\mu} \tag{6.110}$$

the gravity numberGr is described as

$$Gr = \frac{V_{\text{TS}}}{U_0} = \frac{\rho_p d_p^2 g C_c}{18\mu U_0} \tag{6.111}$$

The filter porosity parameter can be described using the solidity, α.

$$A_s = \frac{2 - 2\alpha^{\frac{5}{3}}}{2 - 3\alpha^{\frac{1}{3}} + 3\alpha^{\frac{5}{3}} - 2\alpha^2} \tag{6.112}$$

The van der Waals number, N_{vdw}, is described in terms of Hamaker constantH_{ij}

Table 6.2 Hamaker constants

Particle-media	Hamaker constant (J)	References
Glass beads–Air	5×10^{-19}	[1]
NaCl particles–Air	0.64×10^{-19}	[2]
Silica–Air	0.65×10^{-19}	[13]

$$N_{\mathrm{vdw}} = \frac{4H_{\mathrm{ij}}}{9\pi\mu d_p^2 U_0} \tag{6.113}$$

where H_{ij} = Hamaker constant that characterizes the interaction between aerosol particles and the granule. In general, the Hamaker constant is case-specific and it quantifies the interaction between the airborne particles and the fluids [2]. Three example constants are listed in Table 6.2. Much more of the Hamaker constants of inorganic materials can be found in the paper by Bergstrom [2].

Later on, Tufenkji and Elimelech [35] further improved the granular filtration model by including interception in the simulation of particle motion. The single granule collection efficiency by this new model is described as

$$\begin{aligned}\eta_{\mathrm{sG}} = {} & 2.4A_s^{\frac{1}{3}} Pe^{-0.715} N_{\mathrm{vdw}}^{0.052} \left(\frac{d_p}{d_G}\right)^{-0.081} + 0.55A_s N_A^{\frac{1}{8}} \left(\frac{d_p}{d_G}\right)^{\frac{15}{8}} \\ & + 0.22N_{\mathrm{vdw}}^{0.053} Gr^{1.11} \left(\frac{d_p}{d_G}\right)^{-0.24}\end{aligned} \tag{6.114}$$

where Pe is the particle Peclet number (Pe) and N_A is the attraction number that characterizes the effects of van der Walls attraction and fluid velocity on particle deposition due to interception.

$$N_A = \frac{H_{\mathrm{ij}}}{3\pi\mu d_p^2 U_0} \tag{6.115}$$

While this equation was validated using water filtration, Golshahi et al. [13] found that neither of the single fiber efficiencies is way below the experimental measurements for air filtration. Therefore, by correlating the experimental data for all cases tested, with the TE model Eq. (6.114) using the least square method, they proposed another equation for the single granule efficiency,

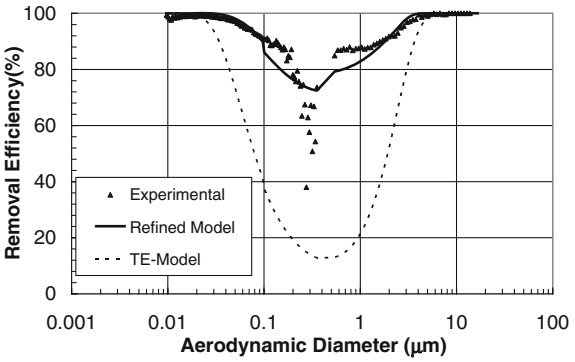

Fig. 6.16 Comparison of the models with the experiments

$$\eta_{sG} = 14A_s^{1/3}Pe^{-0.23}N_{vdw}^{0.052}\left(\frac{d_p}{d_G}\right)^{0.34} + 0.55A_sN_A^{\frac{1}{8}}\left(\frac{d_p}{d_G}\right)^{1.675} + 0.22N_{vdw}^{0.053}Gr^{1.11}\left(\frac{d_p}{d_G}\right)^{-0.24} \quad (6.116)$$

Figure 6.16 shows a comparison between the TE model Eq. (6.114) and the refined model Eq. (6.116) with the experiments. Experiments were conducted using 2-mm glass beads in dry air with a bed thickness of 12.7 cm. The corresponding air flow rate was 65 L/min [13].

In granular filtration, particles are collected as they pass through a bed of granules by the same mechanisms that operate in a fibrous filter. In air cleaning, granular filtration is used primarily for sticky, corrosive, or high-temperature particles. Sometime, granules are driven to move for circulation, regeneration, and/or low resistance to air flow.

6.6 Practice Problems

1. The size distribution and collection efficiency of a particle separator as a function of particle size is shown in the table below. Estimate the cut size and the overall collection efficiency of the control device.

Particle size range (μm)	Mass fraction	Efficiency (%)
0–20	0.11	15
20–40	0.25	25
40–60	0.35	50
60–80	0.19	75
80–100	0.10	100

2. An industrial plant is using cyclone and electrostatic precipitator in serial for air emission control. A cyclone has an 80 % efficiency and it is followed by an electrostatic precipitator. The inlet air to the cyclone has a dust load of 150 g/m^3. What are the collection efficiency of the electrostatic precipitator and the allowable concentration of fly ash in the air that exits from the electrostatic precipitator, in order for the whole system to meet the total collection efficiency of 99 %?
3. Find the precipitation velocity of a 1 μm particle between two parallel plates with a potential difference of 1000 V. The distance between the two plates is

0.01 m and the particle has 100 element charges. The electrical mobility of the particle with a single charge is 1.1×10^{-9} m^2/Vs.

4. A 2 mm thick home furnace filter is made of fiberglass with 3 % solidity. The average diameter of the fiber is 20 μm. The filter is perpendicular to the face airflow of 1.5 m/s. Assume standard room conditions and neglect the electrostatic effect, determine the filter efficiency without circulation for particles of 5 μm in aerodynamic diameter.
5. A 98 % efficient electrostatic precipitator removes fly ash from combustion gases flowing at 10,000 m^3/min. Calculate the required collection area, for an effective precipitation velocity of 5.5 m/min.

Particle size range (μm)	Mass percent in size range
0–2	10
2–12	20
12–20	25
20–40	25
40–70	15
70–100	5

6. A wire-tube electrostatic precipitator has a wire diameter of 5 mm and a tube diameter of 50 cm. The potential between the wire and the cylinder is 5000 V. What is the electrical field intensity at 200 mm radial position?
7. An electrostatic precipitator has a total collection plate area of 5,500 m^2 and treats 8,000 m^3/min of air. If the effective drift velocity is 6 m/min, calculate the actual collecting efficiency.
8. Calculate the overall collection efficiency of a conventional Lapple cyclone with inlet height of 1 m and width of 0.5 m. Air enters the cyclone with a flow rate of 250 m^3/min. The density of particles flowing through the cyclone is 1,500 kg/m^3. The size distribution of the particles is shown in table below.
9. Calculate the cut size diameter of a conventional Lapple cyclone having inlet height of 1 m and width of 0.5 m. The standard air viscosity is 0.0072 kg/m-h. Air flows into the cyclone with a flow rate of 450 m^3/min. The density of particles flowing through the cyclone is 1,200 kg/m^3.
10. Calculate the pressure drop of a conventional Lapple cyclone having inlet height of 0.5 m, width of 0.25 m, and body inner diameter of 0.5 m. The standard air containing particles flow into the cyclone with a flow rate of 150 m^3/min. The density of particles flowing through the cyclone is 1,500 kg/m^3 and K = 16.
11. Calculate the following collection efficiencies of a single fiber per unit volume in a filter for particles of 8 μm in aerodynamic diameter under standard density and neglecting electrostatic effect. The filter bulk thickness is 5 mm, its solidity is 5 %. The average diameter of the fiber is 25 μm. The face velocity is 2 cm/s.

a. collection efficiency by interception
b. collection efficiency by inertial impaction
c. collection efficiency by diffusion
d. overall fiber collection efficiency

12. Calculate the pressure drop across the filter described in problem 11 above under standard condition.

References and Further Readings

1. Attard P, Schulz JC, Rutland MW (1998) Dynamic surface force measurement. I. van der Waals collisions. Rev Sci Instrum 69:3852–3866
2. Bergstrom L (1997) Hamaker constants of inorganic materials. Adv Colloids Interface Sci 70:125–169
3. Brown R (1993) Air filtration: an integrated approach to the theory and applications of fibrous filters. Pergamon, Oxford
4. Cooper CD, Alley FC (2002) Air pollution control—a design approach, 3rd edn. Waveland Press, Inc., Long Grove
5. Corbin RG (1987) A method for the location of sparks in electrostatic precipitators. Appl Acoust 22:297–317
6. Crawford M (1976) Air pollution control theory. McGraw-Hill Book Company, New York
7. Rubenstein DI, Koehl MAR (1977) The mechanisms of filter feeding: some theoretical considerations. Am Nat 111(981):981–994
8. Davies CN (ed) (1973) Air filtration. Academic Press, London
9. Dirgo J, Leith D (1985) Cyclone collection efficiency: comparison of experimental results with theoretical predictions. Aerosol Sci Technol 4:401–415
10. Engelbrecht HL (1981) Rapping systems for collecting surfaces in an electrostatic precipitator. Environ Int 6:297–305
11. Flagan R, Seinfeld JH (2012) Fundamentals of air pollution engineering. Dover Publications Inc., New York
12. Gauthier TA, Briens CL, Bergougnou MA, Galtier P (1990) Uniflow cyclone efficiency study. Powder Technol 62:217–225
13. Golshahi L, Abedi J, Tan Z (2009) Granular filtration for airborne particles—correlation between experiments and models. Can J Chem Eng 87(5):726–731
14. Goncalves JAS, Alonso DF, Costa MAM, Azzopardi BJ, Coury JR (2001) Evaluation of the models available for the prediction of pressure drop in venturi scrubbers. J Hazard Mater B 81:123–140
15. Hinds W (1998) Aerosol technology. Wiley & Sons, New York
16. Jiao J, Zheng Y (2007) A multi-region model for determining the cyclone efficiency. Sep Purif Technol 53:266–273
17. Kirsh AA, Fuchs NA (1968) Studies of fibrous filters—III: diffusionsal deposition of aerosol in fibrous filters. Ann Occup Hyg 11:299–304
18. Kuwabara S (1959) The forces experienced by randomly distributed parallel circular cylinders or spheres in viscous flow at small Reynolds numbers. J Phys Soc Japan 14(4):527–532 (in English)
19. Lapple CE (1951) Processes use many collector types. Chem Eng 58:144–151
20. Lee KW, Liu BYH (1982) Theoretical study of aerosol filtration by fibrous filters. Aerosol Sci Technol 1(2):147–161
21. Leith D, Mehta D (1972) Cyclone performance and design. Atmos Environ 7:529–549

22. Leith D, Licht W (1972) Collection efficiency of cyclone type particle collectors, a new theoretical approach. AIChE Symp Ser: Air-1971 68:196
23. Maloney JO, Wilcox AC (1950) Centrifugation bibliography, engineering bulletin, No. 25. University of Kansas Publications, Lawrence
24. Ogawa A, Sugiyama K, Nagasaki K (1993) Separation mechanism for fine solid particles in the uniflow type of the cyclone dust collector. In: Paper presented at Filtech Conference, Horsham, West Sussex, UK, pp. 627–640
25. Ozis F, Singh M, Devinny J, Sioutas C (2004) Removal of ultrafine and fine particulate matter from air by a granular bed filter. J Air Waste Manag Assoc 54:935–940
26. Perkins HC (1974) Air pollution, International student edn. McGraw-Hill, Kogakusha
27. Pushnov AS (2006) Calculation of average bed porosity. Chem Pet Eng 42:14–17
28. Qian F, Zhang J, Zhang M (2006) Effects of the prolonged vertical tube on the separation performance of a cyclone. J Hazard Mater 136:822–829
29. Quevedo J, Patel G, Pfeffer R, Dave R (2008) Agglomerates and granules of nanoparticles as filter media for submicron particles. Powder Technol 183:480–500
30. Rajagopalan R, Tien C (1976) Trajectory analysis of deep-bed filtration with the spherein-cell porous media model. AIChE J 22:523–533
31. Spielman L, Goren SL (1968) Model for predicting pressure drop and filtration efficiency in fibrous media. Environ Sci Technol 2:279–287
32. Summer RJ, Briens CL, Bergougnou MA (1987) Study of a novel uniflow cyclone design. Can J Chem Eng 65:470–475
33. Tan Z (2008) An analytical model for the fractional efficiency of a uniflow cyclone with a tangential inlet. Powder Technol 183(2):147–151
34. Tien C, Ramarao BV (2007) Granular filtration of aerosols and hydrosols, 2nd edn. Elsevier, Oxford
35. Tufenkji N, Elimelech M (2004) Correlation equation for predicting single collector efficiency in physicochemical filtration in saturated porous media. Environ Sci Technol 38:529–536
36. Wu MS, Lee K-C, Pfeffer R, Squires AM (2005) Granular-bed filtration assisted by filter cake formation 3. Penetration of filter cakes by a monodisperse aerosol. Powder Technol 155:62–73
37. Xiang R, Park SH, Lee KW (2001) Effects of cone dimension on cyclone performance. J Aerosol Sci 32:549–561
38. Yeh HC, Liu BYH (1974) Aerosol filtration by fibrous filters—I. Theoretical. J Aerosol Sci 5:191–204
39. Yeh HC, Liu BYH (1974) Aerosol filtration by fibrous filters—II. Experimental. J Aerosol Sci 5:205–217
40. Zhao B (2005) Development of a new method for evaluating cyclone efficiency. Chem Eng Process 44:447–451
41. Pui D, Fruin S, McMurry P (1988) Unipolar diffusion charging of ultrafine aerosols. Aerosol Sci Technol 8:173–187
42. Tan Z (2004) Mechanisms of particle separation in aerodynamic air cleaning, PhD dissertation, University of Illinois at Urbana-Champaign, Illinois, USA